Physical Layer Design Towards VHF Data Exchange (VDE) Link

R. Raulefs, T. A. Stenbock, A. Dammann, S. Plass

German Aerospace Center (DLR)
Institute of Communications and Navigation
Wessling, Germany

I. Introduction

Towards the overall concept of e-navigation by the International Maritime Organization (IMO), one key element is a new communication system, namely VHF Date Exchange System (VDES). VDES consists of the already existing Automatic Identification System (AIS), Application-Specific Messaging (ASM) and the new to be developed VHF Data Exchange (VDE) link. Currently, an international standard is being developed by the International Association of Marine Aids to Navigation and Lighthouse Authorities (IALA) and the International Telecommunication Union (ITU). The maritime community recognizes the concept of VDES as an answer to the following problems: During the last decade the usage of AIS increased and the AIS capacities are highly stressed. Furthermore, new applications are planned to be introduced to the maritime world such as Maritime Safety Information (MSI) services, vessel shore reporting, real-time hydrographic and environmental information services and ice navigation services. These services also increase the appetite for bandwidth. Currently, the definition of Global Maritime Distress and Safety System (GMDSS) is more than 25 years old and is under way of being revised including new emerging needs. Additionally, communication capacities are not globally available. The Polar Regions are cut off from geostationary satellite data pipelines. There is only a minor terrestrial and satellite communications infrastructure existing, which is contrary to increasing activities (mining, cargo, tourism) due to climate change in these challenging areas. The VDE link is part of VDES. This link contains a terrestrial component (VDE-TER) and a satellite component (VDE-SAT). Therefore, VDE will have a global coverage including bidirectional communication capabilities. Within this paper, current results towards the design of the physical layer for VDE-TER and VDE-SAT will be investigated.

II. VDE System

The VDE system aims for concurrent usage of the terrestrial and the satellite downlink signal partially in the same spectrum. Figure 1 shows the channel plan that is currently proposed by IALA to the ITU WG 5B and for the world radio conference (WRC'15) in 2015. The concurrent usage aims to prioritize the terrestrial link within the protocol where the terrestrial base stations on the shore are available. However, the terrestrial system needs to be robust enough to overcome the interference caused by the satellite system.

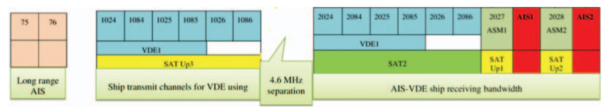

Figure 1: The spectrum allocation of the future VHF data exchange system proposed by IALA.

III. System Model

For our analysis we present the system model of two different schemes. The first one is multi-carrier OFDM and the second is single-carrier square-root raised cosine pulse train. The block diagrams of the two schemes can be seen in Fig. 2a and Fig. 2b:

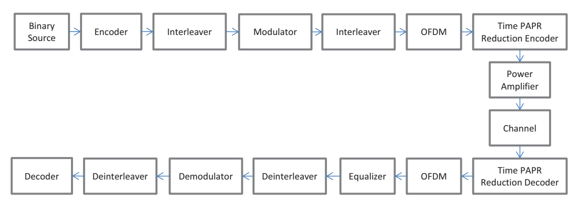

(a) OFDM scheme

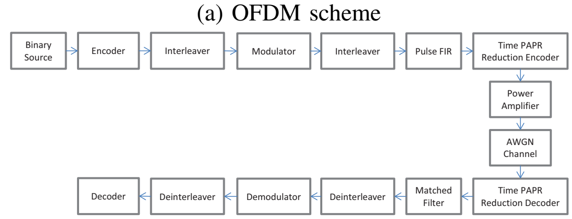

(b) Pulse Train scheme

Figure 2: Block diagram of simulation schemes

A. OFDM

Orthogonal Frequency-Division Multiplexing (OFDM) modulates N data symbols $s[k]$ onto individual frequency separated N subcarriers with low symbol rate. To generate an OFDM symbol, the Inverse Fast Fourier Transform (IFFT) is

978-0-933957-43-5

used on the modulated data symbols to create the time-domain OFDM waveform samples:

$$S[n] = \frac{1}{\sqrt{NT_s}} \sum_{k=0}^{N-1} s[k] e^{j2\pi \frac{nk}{N}} \tag{1}$$

where N is the number of subcarriers, $s[k]$ is the modulated symbols, and T_s is the sampling interval. The scaling factor $1/\sqrt{NT_s}$ is needed to maintain the normalized energy per transmitted sample. To prevent inter-symbol interference (ISI) between OFDM symbols, a cyclic prefix (CP) is added as an overhead to artificially introduce a circular convolution as the time-domain signal is transmitted over the channel:

$$\underbrace{S[N-N_{cp}], ..., S[N-1]}_{\text{Cyclic Prefix}}, \underbrace{S[0], z[1], ..., S[N-1]}_{\text{Normal OFDM symbol}} \tag{2}$$

where the CP is a copy of the last N_{cp} samples of the original OFDM symbol. A requirement of the CP is that the length is greater than the expected channel delay spread or otherwise ISI will occur.

We consider different modulation schemes to map the coded bits to complex by quadrature amplitude (QAM) modulation or amplitude-phase-shift-keying (APSK). The serial sequence of N complex data symbols are multiplexed in parallel onto subcarriers and perform an IFFT and add the CP. A resulting waveform after an OFDM modulation of 32 subcarriers with 16QAM complex symbols on each subcarrier, and an FFT length of 256 can be seen in Fig. 3:

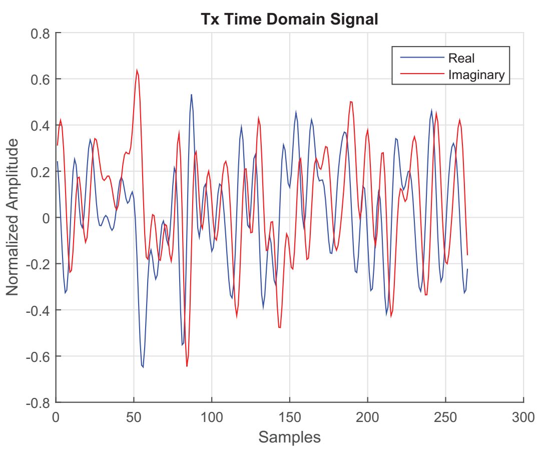

Figure 3: Plain time-domain OFDM signal

Due to the fact that the transmitter side simply performs an IFFT on the modulated symbols as seen in equation 1, the opposite is done to regain the modulated symbols on the receiver from the incoming signal:

$$y[n] = z[n] * h[n] + w[n] \tag{3}$$

$$r[k] = \sum_{n=0}^{N-1} y[n] e^{\frac{-j2\pi kn}{N}} = H[k]s[k] + w[k] \tag{4}$$

where $H[k]$ is the frequency-domain complex channel gain, $w[k]$ is added noise, and $r[k]$ is the modulated symbols $s[k]$ distorted by the channel.

To remove the channel distortion the data symbols are multiplied by the estimated complex channel fading coefficients.

B. Square-root raised cosine pulse train

Modulated data symbols can be pulse shaped so that the transmitted signal suits the communication channel and importantly create waveforms within the limited spectrum mask.

To prevent ISI, pulses are to be designed such that at every sampling interval, all pulses except one has zero crossings. The raised cosine pulse fulfills this requirement as it is a Nyquist pulse. However, with the use of a matched filter on receiver side, the net response of both the transmitter and receiver filters must be considered and this leads to that the square-root raised cosine (SRRC) pulses should be used for pulse shaping the information symbols.

The FIR filter in Fig. 2b have coefficients of a SRRC pulse and when the modulated data symbols are convolved with the filter, a waveform consisting of a superimposed train of pulses is the result. We generate SRRC coefficients by:

$$v(t) = \frac{sin(\frac{\pi(1-\beta)t}{T_s}) + \frac{4t\beta}{T_s} cos(\frac{\pi(1+\beta)t}{T_s})}{\frac{\pi t}{T_s}(1 - \frac{16\beta^2}{T_s^2} t^2)} \tag{5}$$

where β is the roll-off factor and T_s is the sampling interval. The roll-off factor has an important role in the creation of SRRC coefficients. It determines how much excess bandwidth the pulse should occupy. Naturally, the lower the roll-off factor, the less excess bandwidth is used but also more time is required to send the pulse hence lowering throughput. The relationship between the roll-off factor, the symbol rate and the bandwidth is expressed as:

$$R_s = \frac{2}{T_s(1+\beta)} = \frac{2f_s}{1+\beta} \tag{6}$$

where f_s is the sampling frequency and bandwidth of the system. Fig. 4 and Fig. 5 shows the effects of the roll-off factor in both time and frequency domain:

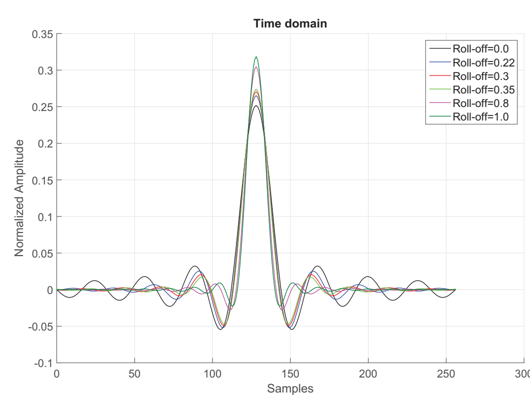

Figure 4: Time domain Square-Root Raised Cosine pulses

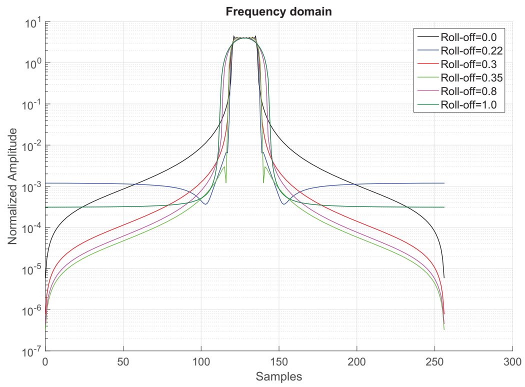

Figure 5: Frequency domain Square-Root Raised Cosine pulses

Consider incoming complex 16-QAM symbols being pulse shaped in the SRRC FIR filter. The output of the FIR filter can be expressed as:

$$s(t) = \sum_{k=0}^{\infty} a_k v(t - kTs) = a_0 v(t) + a_1 v(t - kT_s) + \ldots \quad (7)$$

where $v(t - kT_s)$ is the pulse used to pulse shape the k'th symbol a_k. A resulting waveform can be seen in Fig. 6 where 32 16QAM symbols are pulse shaped through a SRRC FIR filter with a roll-off factor of 0.3:

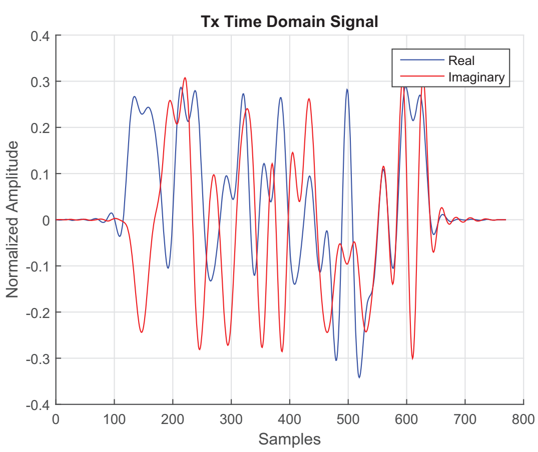

Figure 6: Plain time domain pulse-train signal

C. Matched filter

To get some background of the main idea behind the matched filter is that it attempts to minimize the error energy of incoming pulses. If the error between the i'th signal pulse $s_i(t)$ and the received signal $y(t)$ is to be minimized, the error can be defined as:

$$e_i(t) = |y(t) - s_i(t)| \quad (8)$$

and using the definition of signal energy, the error energy can be defined:

$$E_{e_i} = \int_{-\infty}^{\infty} |y(t) - s_i(t)|^2 dt \quad (9)$$

The problem that a matched filter has to solve is to find which signal pulse gives the lowest error energy:

$$\hat{s}_i(t) = arg \min_i \left[\int_{-\infty}^{\infty} [y(t) - s_i(t)]^2 dt \right] \quad (10)$$

and with some basic arithmetic simplification, $\hat{s}_i(t)$ can be simplified:

$$\hat{s}_i(t) = arg \max_i \left[\int_{-\infty}^{\infty} [y(t) s_i(t)] dt - \frac{E_{e_i}}{2} \right] \quad (11)$$

and using a normalized signal pulse when pulse shaping, the energies of the pulses become $E_{s_1} = E_{s_2} = \ldots = E_{s_i}$ and the final problem to be solved by the matched filter can be even further simplified:

$$\hat{s}_i(t) = arg \max_i \left[\int_{-\infty}^{\infty} [y(t) s_i(t)] dt \right] \quad (12)$$

meaning that if matched correctly, $\hat{s}_i(t) \approx s_i(t)$ and a simple decision can be made.

With the background of what the matched filter is trying to achieve, consider a received signal from the channel $y(t)$ that is to go through the matched filter $v(-t)$, and the result is basically just the convolution:

$$z(t) = y(t) * v(-t) \quad (13)$$

Assuming the error is negligible for the sake of simplicity, $y(t) \approx s(t)$ where $s(t)$ is transmitted signal as seen in equation (7). Combining this assumption and equation (13), the matched filter result can be expressed as:

$$\begin{aligned} z(t) &= s(t) * v(-t) \\ &= \sum_{k=0}^{\infty} a_k \int_{-\infty}^{\infty} v(t - kTs) v(\tau - t) d\tau \end{aligned} \quad (14)$$

This might not be very intuitive to see but if the output of the matched filter is sampled at the correct interval of T_s, the sample will have the amplitude of a_k. This can be shown with the following example. Consider that we sample the matched filter output at Ts, in other words $z(t = Ts)$:

$$z(t=T_s) = a_0 \int_{-\infty}^{\infty} v(\tau)v(\tau - T_s)d\tau$$
$$+a_1 \int_{-\infty}^{\infty} v(\tau - T_s)v(\tau - T_s)d\tau$$
$$+a_2 \int_{-\infty}^{\infty} v(\tau - 2T_s)v(\tau - T_s)d\tau + ...$$

Then due to the fact that all pulses are zero at kT_s except at $v(T_s)$, all integrals results in:

$$\begin{aligned} z(t=T_s) &= 0 + a_1 \int_{-\infty}^{\infty} v(\tau - T_s)v(\tau - T_s)d\tau + 0 + ... \\ &= a_1 \int_{-\infty}^{\infty} v(\tau - T_s)v(\tau - T_s)d\tau \\ &= a_1 \int_{-\infty}^{\infty} v(\tau - T_s)^2 d\tau \\ &= a_1 E_v \end{aligned}$$

and since the energy of the pulse can be normalized, the equation can be simplified even further:

$$z(t=T_s) = a_1 \tag{15}$$

Similarly, $z(t = kT_s) = a_k$ can be proved and hence it is shown that if sampled at the correct time, the matched filter allows for recovery of the symbols from the transmitted pulse train waveform, and the output of the matched filter can be used for further processing.

D. PAPR Reduction Techniques

One major drawback of OFDM is that the Peak-to-Average-Power Ratio (PAPR) can become significantly large and the need for expensive power amplifiers must be used. As can be seen in Fig. 3, there are many large peaks compared to the average power and to compensate for high PAPR, a few PAPR reduction techniques are implemented, both for OFDM and pulse-train schemes. Just before the time-domain waveform is amplified by the power amplifier, the signal goes through a PAPR reduction encoding block. For some PAPR reduction techniques, the effects can be reversed which is done in the PAPR reduction decoder block. In the simulations, the PAPR reduction can perform two different techniques: clipping and companding transforms.

1) Clipping: Clipping is one of the simplest methods of preventing high peaks in a signal. The signal envelop will be limited to a set Clipping Level (CL) where if the signal exceeds the CL, it will be clipped and if it does not exceed the CL, it will be untouched. In the simulations, the CL will be calculated based on a Clipping Ratio (CR) which takes into effect the average of the signal:

$$CR = 20\log_{10}\left(\frac{CL}{E[x[n]]}\right) \tag{16}$$

When the clipping ratio is set to 1dB and 5dB, resulting 16QAM OFDM signals can be seen in Fig. 7 and Fig. 8 respectively:

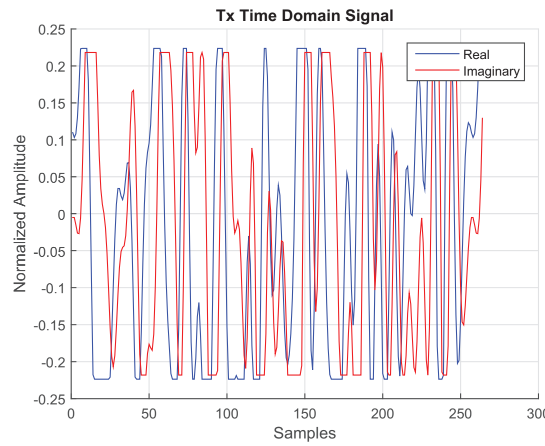

Figure 7: Resulting 16QAM OFDM signal (CR = 1 dB)

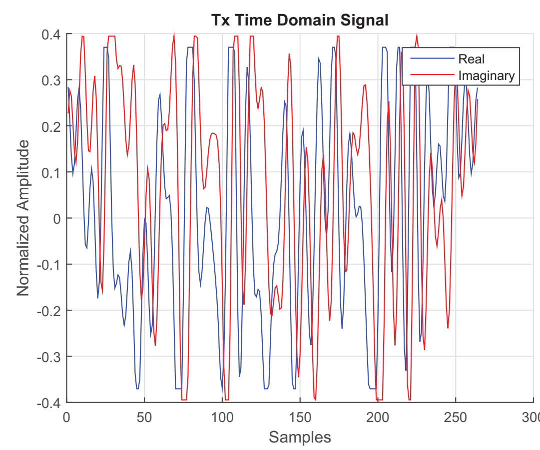

Figure 8: Resulting 16QAM OFDM signal (CR = 5 dB)

It can be seen that having a lower value of the CR, the PAPR will be reduced. However, the signal will be severely distorted.

2) Companding Transforms: Companding transforms attempts to lower PAPR by increasing the average power instead of reducing the peak power. In the simulation, three companding transforms are considered: linear symmetrical transforms (LST), nonlinear asymmetrical transforms (NLAST), and nonlinear symmetrical transforms (NLST). A profile of each transform is shown in Fig. 9:

LST is simply tranforming the input x according to the formula:

$$C_{LST}(x[n]) = ax[n] + b \tag{17}$$

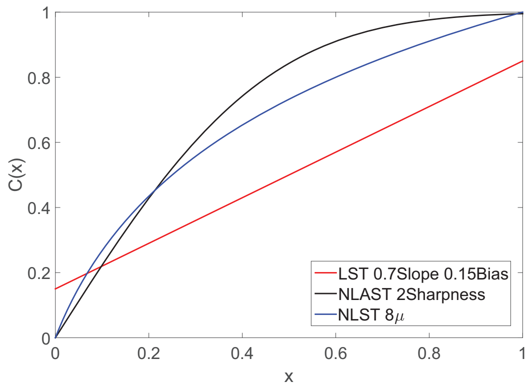

Figure 9: Companding transforms profiles

where $0 < a < 1$ and $0 < b$. Depending on the need of the system, a and b can be set accordingly but the transform will always be linear.

Compared to LST, NLAST provides a transform where lower signal values are affected more than the higher signal values. NLAST transforms the input by using the error function given by:

$$C_{NLAST}(x[n]) = k_1 \text{erf}\left(k_2 x[n]\right) \tag{18}$$

where k_1 is a multiplication factor, and k_2 is the sharpness of the "bend" of the curve. In the simulation, k_1 is set to $\max(x[n])$ to maintain the range of the signal envelope to be the same as original $x[n]$.

One issue with NLAST is that it also affects above average signal values significantly. This can be seen in Fig. 9 where the transform for input values above 0.5 gets transformed to a much higher value (ie. $C(0.6) \approx 0.9$). NLST provides a transform that preserves higher values much better than NLST but also has good effects on lower signal values. NLAST uses the μ-law to transform the signal, which is expressed as:

$$C_{NLST}(x[n]) = \frac{A \ \text{sgn}(x[n]) \log_{10}(1 + \mu \left|\frac{x[n]}{A}\right|)}{\log_{10}(1 + \mu)} \tag{19}$$

where A is the normalization factor such that $0 < \left|\frac{x[n]}{A}\right| < 1$ and μ is the companding parameter. In the simulation, A is chosen to be $\max(x[n])$. A resulting 16QAM OFDM waveform can be seen in Fig. where NLST with a μ of 8 has been applied:

On the receiver side, the μ-law can be reversed to recover the original signal using the inverse μ-law equation:

$$x[n] = A \frac{\exp\left[\frac{C(x[n])}{A \ \text{sgn}(C(x[n]))} \log(1 + \mu)\right] - 1}{\mu \ \text{sgn}(C(x[n]))} \tag{20}$$

which is computed in the PAPR reduction decoder block.

E. Modulation

The system supports three modulation schemes: M-QAM, M-PSK, and M-APSK.

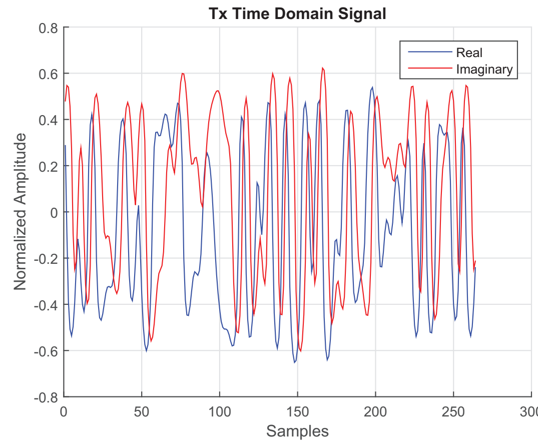

Figure 10: Resulting 16QAM OFDM signal after NLST ($\mu = 8$)

1) M-QAM: Quadrature Amplitude Modulation is widely used in many communication systems and is also supported in the modulation and demodulation blocks in the simulations. M in this case denotes how many points are in the modulation schemes the symbol can be represented as. $log_2(M)$ is effectively the number of bits that can be modulated into one single symbol. QAM symbols can take on many different phase and amplitude values. In the simulations, the bit mapping is Gray mapping. An example of a 16QAM modulation scheme is seen in Fig. 11:

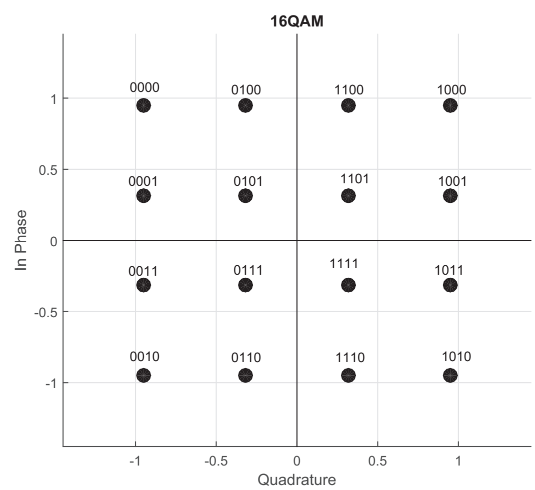

Figure 11: Gray mapped 16QAM

2) M-PSK: Phase-Shift Keying modulates symbols to different phases only, there's no change in amplitude between the possible modulation points. Similar to QAM, the bit mapping is Gray mapping. An example of 16PSK is seen in Fig. 12:

3) M-APSK: Amplitude and Phase-Shift Keying combines the functionality of QAM and PSK by modulating bits to symbols with varying amplitude and phase. Although QAM also modulates to varying amplitudes and phases, APSK

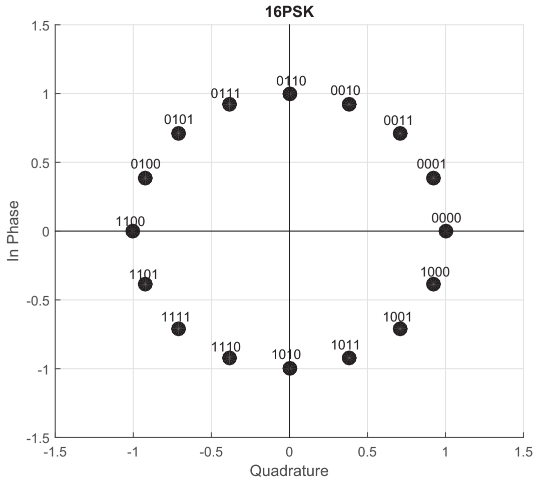

Figure 12: Gray mapped 16PSK

provides a great advantage by allowing less possible amplitude levels for the same number of bits per symbol. This advantage gives it applicability in systems where power control is of great essence, such as satellite systems.

The simulations can use two different bit mapping version of APSK. First, a regular scheme with an arbitrary number of rings and symbols per ring, with Gray mapping, can be used. Second, the symbols can be generated according to the Second generation Digital Video Broadcasting (DVB-S2) standard [1]. 16APSK as defined by DVB-S2 standard is seen in Fig. 13:

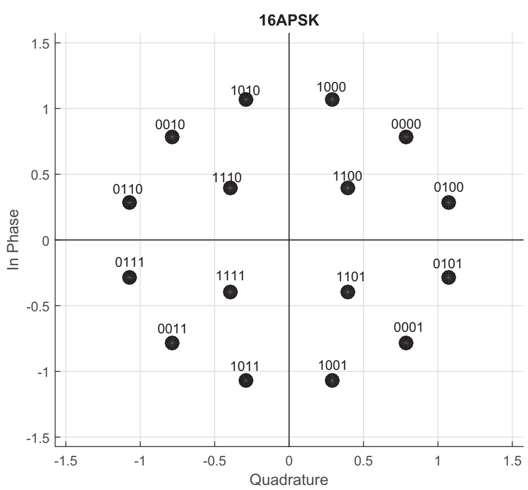

Figure 13: DVB-S2 16APSK

F. Power Amplifier Models

In the simulations, a waveform goes through a power amplifier before being transmitted over the channel. Power amplifiers are a common cause for nonlinearity in systems and to see the effects of them on the signal in the simulations, three common memoryless and frequency-nonselective power amplifier models are implemented: Linear, Solid State Power Amplifier (SSPA), and Traveling Wave-Tube Amplifier (TWTA).

The models are based on the same concept that the input is considered as:

$$x(t) = |x(t)|e^{j\phi(t)} \tag{21}$$

where the $|x(t)|$ is the amplitude of the input signal and $\phi(t)$ is the phase of the input signal. The output is then expressed as:

$$y(t) = G\left[|x(t)|\right] e^{j\{\phi(t)+\Phi(|x(t)|)\}} \tag{22}$$

where $G[.]$ is the amplitude/amplitude (AM/AM) conversion and $\Phi(.)$ is the amplitude/phase (AM/PM) conversion.

For the linear power amplifier model, the input signal amplitude is simply multiplied with a gain. This is impossible in real systems but is implemented into the simulations.

Similar to the linear power amplifier model, The SSPA model only affects the amplitude of the input signal meaning $\Phi(|x(t)|) = 0$. However, it is not linear in output amplitude which can be determined according to:

$$G[|x(t)|] = \frac{g_0|x(t)|}{\left[1 + \left(\frac{|x(t)|}{x_{sat}}\right)^{2p}\right]^{\frac{1}{2p}}} \tag{23}$$

where g_0 is the amplifying gain, x_{sat} is the saturation point of the amplifier, and p is the AM/AM sharpness in the saturation region.

The TWTA model affects both the signal output amplitude and phase. It is expressed as:

$$G[|x(t)|] = \frac{\alpha_a|x(t)|}{1 + \beta_a|x(t)|^2} \tag{24}$$

$$\Phi[|x(t)|] = \frac{\alpha_\phi|x(t)|}{1 + \beta_\phi|x(t)|^2} \tag{25}$$

where α_a, β_a controls the characteristics of the AM/AM conversion and α_ϕ, β_ϕ controls the characteristics of the AM/PM conversion [2].

For the simulations, the choice of the TWTA parameters α_a, β_a, α_ϕ, β_ϕ are be set to common values, according to Rahmatallah amd Mohan, such that [**?**]:

$$\alpha_a = 2x_{sat}, \beta_a = \frac{1}{x_{sat}^2}, \alpha_\phi = \frac{\pi}{12}, \beta_\phi = 0.25 \tag{26}$$

Fig. 14 shows the input power and output power relation between the three power amplifier models with $g_0 = 2$, $x_{sat} = 2$, and a sharpness of the SSPA of $p = 2$:

The nonlinear effect of the power amplifiers can be seen in Fig. 15 where the signal is clearly distorted:

IV. Results and Discussions

A. OFDM over Maritime Channels

For our analysis we applied the gunfleet channel model that we derived from the ITU report about a VHF channel sounding campaign [3]. The proposed channel model contains a significant path by line of sight, and a second signal path

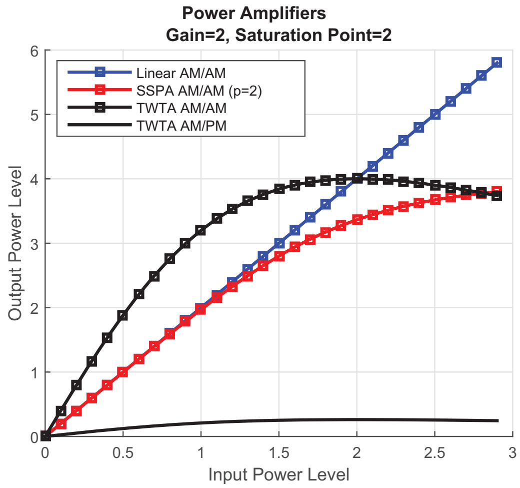

Figure 14: Comparison between input/output relation of Linear, SSPA, and TWTA power amplifier models

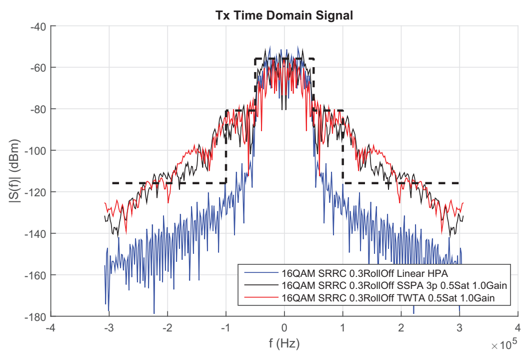

Figure 15: Comparison between Linear, SSPA, and TWTA power amplifier model nonlinear effect on signals

coming from a neighboring windmill. Our objective was to understand how much margin the terrestrial downlink system could cope with to derive from this the buffer for the satellite downlink. The maritime radio channel offers some diversity that could be exploited by channel codes (we applied Turbo codes). However, this demands two characteristics of the system. First the data needs to be interleaved over many blocks in time. In our analysis we stretched the block length up to 1s which contains multiple of the AIS frames. Second, we introduced multiple antennas to enable transmit diversity by the Alamouti scheme and by introducing Doppler diversity which could offer a benefit for the performance of the system. The performance results in Figure 16 show that the proposed channel model demands a long interleaver in time to exploit time diversity. By introducing diversity schemes we can achieve a similar performance together with shorting the interleaver length. This is advantageous as the system is more robust to the blinding transmissions of the spectrally close neighbouring AIS system [4] (see Figure 1).

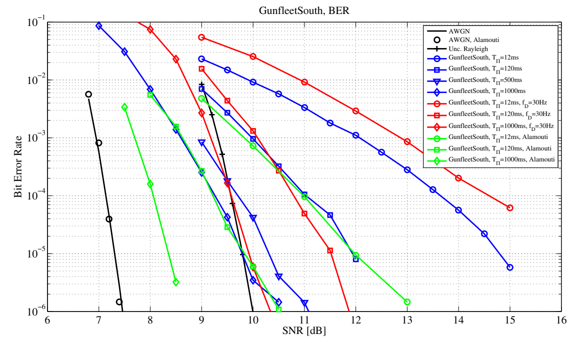

Figure 16: For a channel model derived from the ITU report we investigated the bit error rate for different interleaver lengths of the channel code to exploit time diversity, show the benefits of multiple antennas and compared it as benchmark to the AWGN performance.

B. PAPR Comparison between Pulse Train and OFDM

A key counter argument for OFDM vs. single carrier techniques is the rather high PAPR. This is especially of concern for high power amplifiers (above 10 W). Therefore, we compared the PAPR for different roll-off factors β of the single carrier waveform and different number of subcarriers for OFDM. Fig. 17 shows the performance and outlines in this context the PAPR of the UMTS system (β=0.22) and the TETRA (β=0.35) system. For low number of subcarriers, such as eight, the PAPR is about 1.4 dB for 10 % of the CCDF worse compared to the best roll-off facor of β.

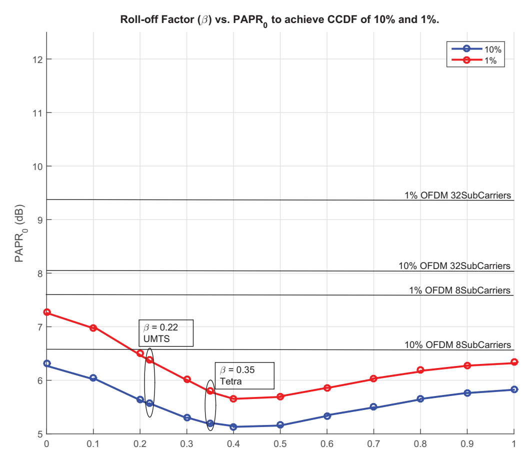

Figure 17: β vs $PAPR_0$ and PAPR values of 8 subcarriers and 32 subcarriers OFDM

V. Conclusions

Enhancing diversity techniques allow long time code bit interleavers with strong channel codes to offer enough margin to cope with a satellite system in parallel. However, for channel codes which need to cope with voice applications a much shorter delay has to be considered. Therefore, artificially enhancing diversity techniques could resolve this even voice communication links. VDES could then also serve as a joint data and voice communication service.

We further investigated the PAPR of single- and multi-carrier systems. The impact of the roll-off factor showed about 1.5 dB worse PAPR compared to a multi-carrier system with only eight subcarriers. The loss could be partially compensated by techniques that shape the signal before the power amplifier to optimize the communication link.

Acknowledgment

The research leading to these results has been carried out under the framework of the project R&D for the maritime safety and security and corresponding real time services. The project started in January 2013 and is led by the Program Coordination Defence and Security Research within the German Aerospace Center (DLR).

References

[1] ETSI, *Digital Video Broadcasting (DVB); Second generation framing structure, channel coding and modulation systems for Broadcasting, Interactive Services, News Gathering and other broadband satellite applications; Part 1: DVB-S2". v1.4.1. 2014-11*, ETSI, 2014.

[2] Seshadri Mohan Yasir Rahmatallah, "Peak-to-average power ratio reduction in ofdm systems: A survey and taxonomy," *IEEE COMMUNICATIONS SURVEYS & TUTORIALS*, vol. 15, November 2013.

[3] Jan Safar, "VHF data exchange system channel sounding campaign," *ITU Report*, vol. Report ITU-R M.2317-0, November 2014.

[4] Francisco Lzaro, Ahmed Hassanin, and Simon Plass, "An advanced AIS receiver using a priori information," in *IEEE Oceans*, Genova, Italy, May 2015.